

---

This is an electronic reprint of the original article.  
This reprint may differ from the original in pagination and typographic detail.

Pulkkinen, Tuija I.; Tanskanen, E.I.; Viljanen, A.; Partamies, N.; Kauristie, K.  
**Auroral electrojets during deep solar minimum at the end of solar cycle 23**

*Published in:*  
Journal of Geophysical Research

*DOI:*  
[10.1029/2010JA016098](https://doi.org/10.1029/2010JA016098)

Published: 01/01/2011

*Document Version*  
Publisher's PDF, also known as Version of record

*Published under the following license:*  
Unspecified

*Please cite the original version:*  
Pulkkinen, T. I., Tanskanen, E. I., Viljanen, A., Partamies, N., & Kauristie, K. (2011). Auroral electrojets during deep solar minimum at the end of solar cycle 23. *Journal of Geophysical Research*, 116(A04207), .  
<https://doi.org/10.1029/2010JA016098>

---

This material is protected by copyright and other intellectual property rights, and duplication or sale of all or part of any of the repository collections is not permitted, except that material may be duplicated by you for your research use or educational purposes in electronic or print form. You must obtain permission for any other use. Electronic or print copies may not be offered, whether for sale or otherwise to anyone who is not an authorised user.

## Auroral electrojets during deep solar minimum at the end of solar cycle 23

T. I. Pulkkinen,<sup>1,2</sup> E. I. Tanskanen,<sup>1</sup> A. Viljanen,<sup>1</sup> N. Partamies,<sup>1</sup> and K. Kauristie<sup>1</sup>

Received 7 September 2010; revised 13 December 2010; accepted 13 January 2011; published 12 April 2011.

[1] We investigate the auroral electrojet activity during the deep minimum at the end of solar cycle 23 (2008–2009) by comparing data from the IMAGE magnetometer chain, auroral observations in Fennoscandia and Svalbard, and solar wind and interplanetary magnetic field (IMF) observations from the OMNI database from that period with those recorded one solar cycle earlier. We examine the eastward and westward electrojets and the midnight sector separately. The electrojets during 2008–2009 were found to be weaker and at more poleward latitudes than during other times, but when similar driving solar wind and IMF conditions are compared, the behavior in the morning and evening sectors during 2008–2009 was similar to other periods. On the other hand, the midnight sector shows distinct behavior during 2008–2009: for similar driving conditions, the electrojets resided at further poleward latitudes and on average were weaker than during other periods. Furthermore, the substorm occurrence frequency seemed to saturate to a minimum level for very low levels of driving during 2009. This analysis suggests that the solar wind coupling to the ionosphere during 2008–2009 was similar to other periods but that the magnetosphere-ionosphere coupling has features that are unique to this period of very low solar activity.

**Citation:** Pulkkinen, T. I., E. I. Tanskanen, A. Viljanen, N. Partamies, and K. Kauristie (2011), Auroral electrojets during deep solar minimum at the end of solar cycle 23, *J. Geophys. Res.*, 116, A04207, doi:10.1029/2010JA016098.

### 1. Introduction

[2] The Sun exhibits long-term variability with roughly 11 year cycles often quantified by the sunspot number ( $R$ ). The “butterfly” diagram of the latitudinal distribution of sunspots shows how the sunspots that early in the solar cycle are generated at high latitudes progressively appear further equatorward toward later phases of the cycle. The latitudinal difference and the changing polarity from one cycle to the next makes it possible to identify sunspots belonging to the ending and beginning cycles, and thus detect the overlaps at the time of cycle change [Weiss and Tobias, 2000].

[3] The last solar minimum was unusually long, and the Sun during the minimum was exceptionally quiet for an extended period [Kirk *et al.*, 2009]. This also led to atypical characteristics of the solar wind with low solar wind speeds and weak interplanetary magnetic field (IMF) magnitude at 1 AU [Lee *et al.*, 2009]. The unusual conditions on the Sun and in the solar wind provide an excellent opportunity to examine the “ground state” properties of the magnetosphere-ionosphere system, and to check whether the low level of driving had an impact on the solar wind-magnetosphere-

ionosphere coupling processes [Gibson *et al.*, 2009]. Cycle 23 finally ended in December 2008, although the solar activity remained very quiet throughout 2009 and the sunspot activity even in 2010 has been unusually low.

[4] The IMAGE magnetometer chain consists of 31 magnetometers ranging in latitude from 58° (Tartu, Estonia) to 79° (Ny-Ålesund, Svalbard), or from 54° to 75° in corrected geomagnetic coordinates [Tanskanen, 2009]. The stations have longitudinal coverage over about 30° from western Norway to the Kola peninsula. The long, continuous and homogeneous time series covering latitudes from subauroral to the polar cap provide a means to monitor the long-term evolution of the auroral ionospheric currents and their variability.

[5] In this paper, we investigate a period consisting of 15 years, covering the period from the minimum at the end of solar cycle 22 through the minimum at the end of cycle 23 (1995–2009). We use the IMAGE chain results to derive the intensity and latitudinal location of the auroral electrojets, and discuss their long-term variability. This variability is associated with simultaneous solar wind and IMF measurements to draw conclusions on the solar wind-magnetosphere-ionosphere coupling processes.

### 2. Solar Activity and Interplanetary Plasma Environment

[6] The monthly sunspot number and  $F_{10.7}$  values provided by the NGDC in Boulder, CO are used to quantify the level of solar activity. The solar wind and IMF data were

<sup>1</sup>Finnish Meteorological Institute, Helsinki, Finland.

<sup>2</sup>Now at School of Electrical Engineering, Aalto University, Espoo, Finland.

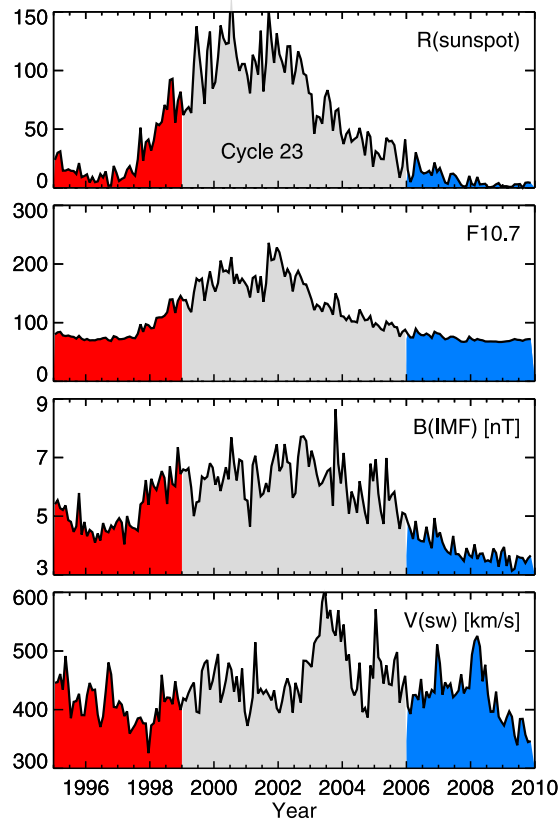


**Figure 1.** Monthly sunspot number, monthly  $F_{10.7}$  flux, monthly average of the interplanetary magnetic field intensity in nT, and monthly average of the solar wind speed in km/s. The 4 year periods around solar minima at the end of cycles 22 and 23 are shown in red and blue, respectively.

obtained from the OMNI-2 database (<http://omniweb.gsfc.nasa.gov/>), which contains hourly averages of the solar wind and interplanetary magnetic field parameters delayed to the average bow shock position. Figure 1 shows the solar activity in terms of monthly values of the sunspot number and  $F_{10.7}$  as well as the IMF magnitude and solar wind speed over the period 1995–2010 covering two minima at the end of cycles 22 and 23, and the maximum of cycle 23. Here we concentrate on two 4 year periods around the minima, 1995–1998 and 2006–2009, marked in Figure 1 by red and blue, respectively.

[7] The minimum after cycle 22 occurred in the summer of 1996, and the solar activity was on the rise from the beginning of 1997. This is in clear contrast with the period 11 years later, when the activity subsided during 2007 after which the Sun remained very quiet with several months of zero sunspot numbers in sequence; the minimum was timed to occur only in December 2008. The solar activity started to increase slowly in 2010 (not shown). Note, however, that the levels of the  $F_{10.7}$  radio flux were not markedly different during the two minima. The IMF magnitude was very weak during the low solar activity in 2008–2009, significantly lower than the values observed during the previous minimum. On the other hand, several high-speed streams during 2008 kept the values of the solar wind speed at least equal to

if not larger than those during the minimum in 1996. Only toward the end of the year 2009 did the solar wind speed decrease to very low values.

### 3. Auroral Electrojet Observations

[8] The IMAGE magnetometer stations record variations in the geomagnetic field at 10 s cadence. The data are processed in a way analogous to the  $AU/AL$  indices to produce local  $IU/IL$  indices [Tanskanen *et al.*, 2002]. While the indices can be computed for all local times, the  $IL$  index has been shown to correlate well with the global  $AL$  index in the local time sector 20–06 MLT, which corresponds to 18–04 UT [Kauristie *et al.*, 1996]. Similarly, the eastward electrojet response to the  $IU$  index is clearly visible only in the dusk sector, roughly 16–20 UT. From the longitudinal chain, we process the properties of the eastward and westward electrojets, in particular the equivalent current maximum current density and total current as well as the latitude of the maximum current density [Amm and Viljanen, 1999; Pulkkinen *et al.*, 2003].

[9] We examine three local time sectors separately: dusk (18–22 LT, eastward electrojet), midnight sector (22–02 LT, westward electrojet) and dawn sector (02–06 LT, westward electrojet). As the local midnight in Scandinavia is at about 2130 UT, the corresponding UT sectors analyzed are 2.5 h earlier of the local times. Figure 2 shows the locations of the

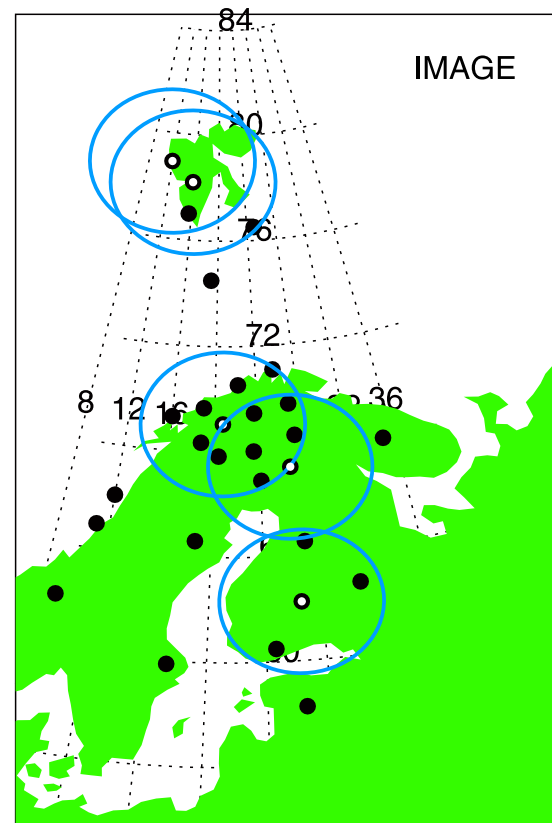


**Figure 2.** Locations of the IMAGE magnetometer stations (black dots) in geographic coordinates. The white dots mark the locations of the all-sky cameras used in this study, and the blue circles illustrate the field of view covered by the imagers.

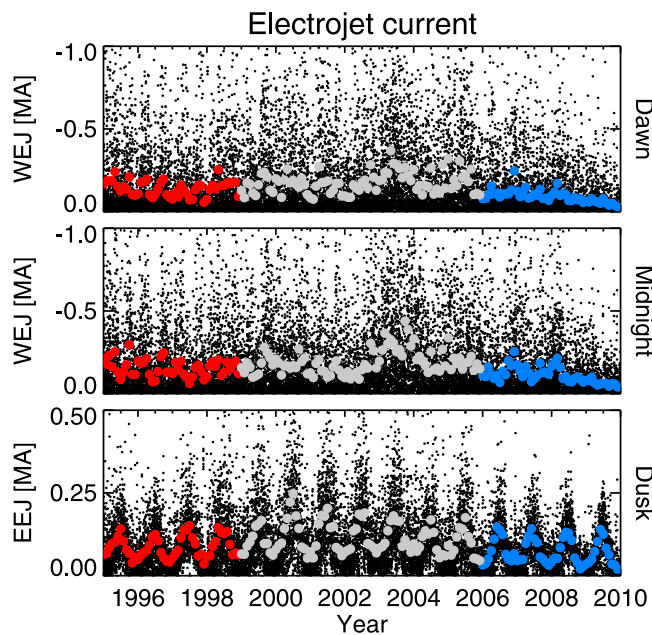


**Figure 3.** Total current in the auroral electrojets in MA in the dawn, midnight, and dusk local time sectors. The black dots show hourly averages, while the large colored and gray dots show monthly averages. The period near the end of cycle 22 is shown in red, while the period near the end of cycle 23 is shown in blue. Note that the westward electrojet is plotted in reversed scale such that the magnitude of the current increases upward. WEJ, westward electrojet (with negative current); EEJ, eastward electrojet (with positive current).

IMAGE magnetometer stations. The coordinates shown are geographic, those will be used throughout the analysis in this paper.

[10] For the statistical analysis, we compute the following averages of the electrojet parameters: For the westward electrojet, we compute the total current, the maximum current density, the central latitude, and the  $IL$  index in the midnight and dawn sectors (22–02 LT, 02–06 LT). For the eastward electrojet, we compute the total current, the maximum current density, the central latitude, and the  $IU$  index in the dusk sector (18–22 LT). Using only data from these local time sectors, we compute hourly, daily and monthly averages.

[11] Figure 3 shows the hourly (small black dots) and monthly (large dots) averages of the auroral electrojet total current intensity during the time periods around the two minima. Each local time sector is shown separately. It is clear that the hourly averages show large variability, but that there are distinct patterns visible in the data. The westward electrojet intensity shows a semiannual variability with maxima in the spring and fall, consistent with the Russell-McPherron effect of geomagnetic activity [Russell and McPherron, 1973]. The eastward electrojet shows strong annual variability with maximum during the summer months and minimum during the winter months. This variability can be associated with the winter-summer asymmetry with higher ionospheric conductivity during the summer months driving larger ionospheric currents [Lyatsky *et al.*, 2001].

Such annual variation is also present in the global  $AE$  indices [Häkkinen *et al.*, 2003]. Note also that the current direction is defined such that the westward current is negative, and it is plotted in a reversed scale with the absolute value of the current intensity increasing upward.

[12] The local time dependence of the westward electrojet is examined in Figure 4. The scatterplots show monthly values of the total westward current and the electrojet central latitude in the midnight and dawn sectors. The plots clearly illustrate that the electrojets in the midnight and morning sectors are highly correlated, but that the electrojet is slightly weaker in the dawn sector especially for higher values of the current, and that the electrojet in the dawn sector is at higher latitudes than it is at local midnight. Moreover, the color coding of the years 1995–1999 in red and years 2006–2009 in blue clearly shows that the electrojets are weaker and at higher latitude during the latter solar minimum period. Examination of the minute and hourly averages reveals high scatter in the correlations (not shown), indicating that the auroral electrojet shape varies as a function of time and geomagnetic activity.

#### 4. Solar Cycle Effects in Auroral Electrojets

[13] A comparison of the electrojet current during the two solar minimum periods is shown in Figure 5. The data are shown as time series from the beginning of 1995 and 2006, which selects similar levels of solar activity at the beginning of the period (1995 and 2006). Note that the minima in Figure 5 do not occur at the same time, the minimum of cycle 22 was reached in the summer of 1996, while the minimum of cycle 23 was only reached at the end of 2008.

[14] Figure 5 (top) shows the sunspot numbers, which are comparable at the beginning of the time series, while they differ quite considerably toward the end of the time series, when cycle 23 had already started to increase after 1997, while cycle 24 did not show any activity through the year 2009. The location of the minima are indicated by the vertical lines. The following six panels show the electrojet current and latitude in the three local time sectors. The gray shadings illustrate the periods of the biannual and annual variations, and are not fitted to the data in any way.

[15] It is clear that both the eastward and westward electrojets have similar intensity at the beginning of both time

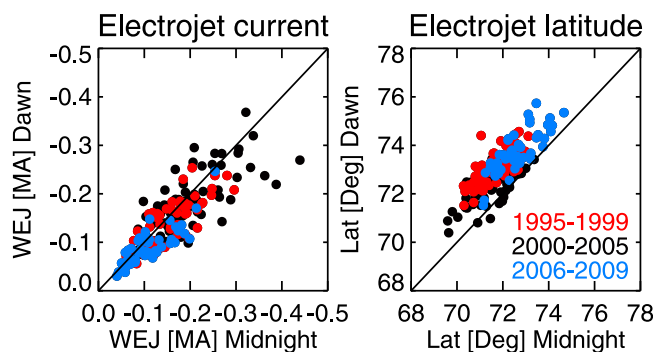


**Figure 4.** Correlation of monthly averages of the total westward electrojet current and the electrojet latitude in the midnight and dawn sectors: 1995–1999 (red), 2000–2005 (black), and 2006–2009 (blue).

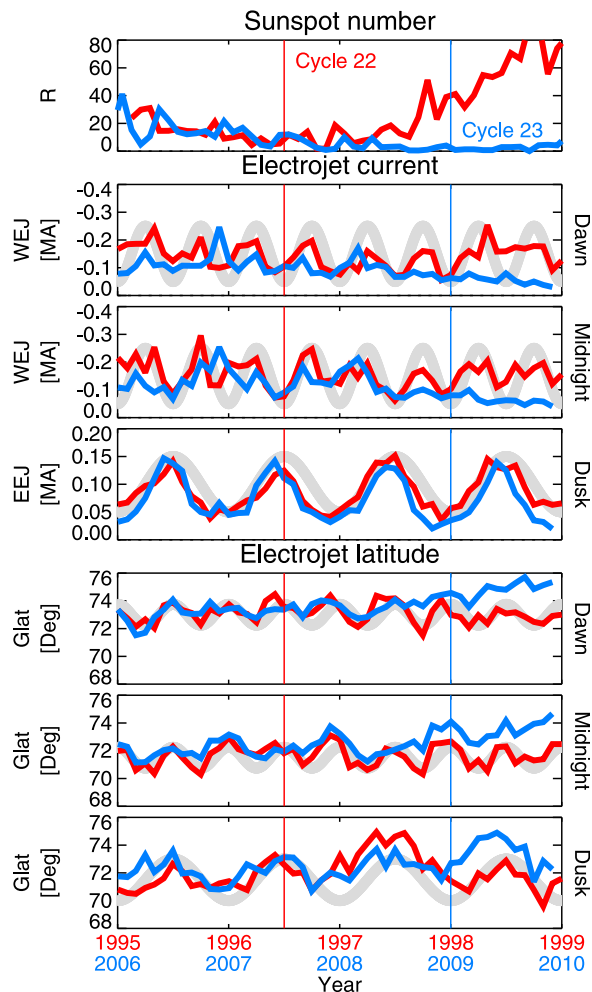


**Figure 5.** Comparison of monthly averages of the electrojet current and latitude. (top) The sunspot number  $R$ ; (middle) the total electrojet current in MA in the dawn, midnight, and dusk sectors; and (bottom) the geographic latitude of the electrojet center in the dawn, midnight, and dusk sectors: 1995–1999 (red) and 2006–2010 (blue). The gray shading shows a constant amplitude biannual (westward electrojet) and annual (eastward electrojet) variation without an attempt to fit the data. The vertical lines mark the times of the solar minima.

series, but that after the minimum the westward electrojet is much weaker from 2008 onward. Furthermore, the semi-annual variation in the westward electrojet is lost almost completely, and the activity is at the level usually obtained during the solstitial periods. On the other hand, the annual variation in the eastward electrojet is intact, and the intensity of the electrojet is only slightly decreased.

[16] The electrojet latitude behavior is very similar to the intensity variations: The latitude during 1995–1999 follows closely the semiannual variation throughout the period in question. The period 2006–2007 follows the same trend, but during the latter part of 2008 and 2009 the semiannual variation in the westward electrojet decreases and the westward electrojet moves poleward. While the annual variation in the eastward electrojet remains during that period, also the eastward electrojet moves to more poleward latitudes.

[17] As already shown in Figure 1, the IMF magnitude was clearly smaller in 2008–2009 than during 1996. Figure 6 shows a comparison of the IMF magnitude, solar wind speed, and the parallel electric field  $E_{PAR} = E \sin(\theta/2)$ , where  $E$  is the magnitude of the solar wind electric field computed as  $-\mathbf{V} \times \mathbf{B}$  and  $\theta$  is the IMF clock angle defined as  $\theta = \tan^{-1}(B_Y/B_Z)$ . The component  $E_{PAR}$  gives the electric field component roughly along the large-scale neutral line at the magnetopause, and thus is a measure of the reconnection efficiency at the dayside magnetopause [Pulkkinen *et al.*, 2009]. The data clearly show that the driving electric field continued to decrease after 2008, such that the driving toward the end of 2009 was at lower level than during the previous minimum in 1996.

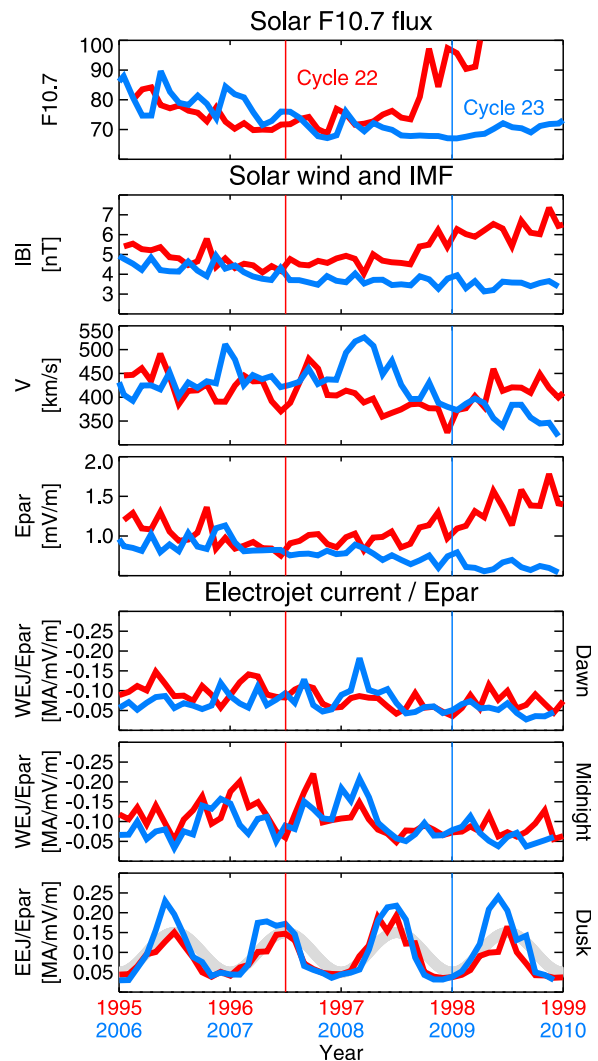


**Figure 6.** Comparison of monthly averages of the electrojet current and latitude. (top) The solar  $F_{10.7}$  flux; (middle) the magnitude of the IMF in nT, the solar wind speed in km/s, and the parallel electric field  $E_{PAR} = E \sin(\theta/2)$  in mV/m; and (bottom) the electrojet currents in the dawn, midnight, and dusk sectors scaled by the parallel electric field: 1995–1999 (red) and 2006–2010 (blue). The gray shading in Figure 6 (bottom) shows a constant amplitude annual modulation without an attempt to fit the data. The vertical lines mark the times of the solar minima.

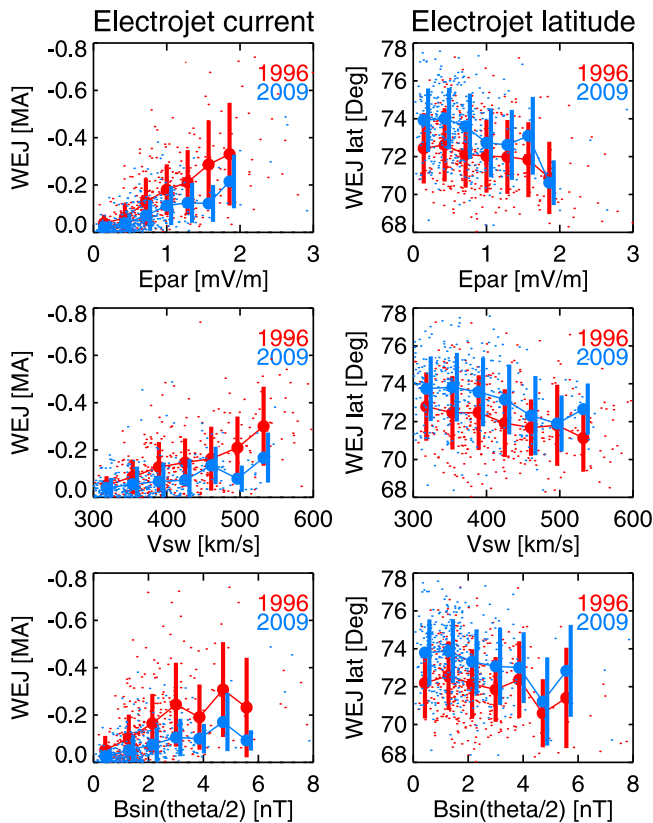


**Figure 7.** Comparison of the daily values of the total electrojet (left) current and (right) latitude in the midnight sector during 1996 (red) and 2009 (blue). The large dots denote binned averages, and the vertical bars give the mean  $\pm 1$  standard deviation in each bin.

[18] Figure 6 (bottom) shows the solar wind-ionosphere coupling efficiency computed by dividing the electrojet current by the driving electric field using hourly averaged values. The westward electrojet scaled by the driving electric field shows some interesting behavior. First, there are large month-to-month variations in the efficiency. Second, it seems that for both solar cycles, and for both dawn and midnight sectors, the average efficiency is slightly higher during the declining phase of the solar cycle (beginning of both time series, 1995–1996 and 2006–2007) than it is for the latter parts of both time series (1997–1999 and 2008–2010). Following the minimum in 1996, the dawn sector efficiency seems to decrease. The decrease one cycle later started at the beginning of 2008, and continued past the minimum throughout 2009.

[19] The efficiency of the eastward electrojet remains constant throughout both periods and is similar for both minima, and the annual modulation is intact. Thus, the solar wind-ionosphere coupling through the eastward electrojet seems to be independent of the solar cycle effects. Furthermore, it is interesting to note that the efficiency of the eastward electrojet is slightly higher than that of the westward electrojet.

[20] Figure 7 examines the driver dependence of the midnight sector westward electrojet latitude and total current on a daily basis. The averaged values of the current (left) and latitude (right) over the few hours the magnetometer

chain spends daily in the local midnight sector are shown in red for the year 1996 at the solar minimum of cycle 22 and in blue for the year 2009 when the solar activity was at its lowest. The latitude and current are shown as function of the driving electric field  $E_{PAR}$  (top), solar wind speed (middle), and the magnetic field magnitude multiplied by the factor  $\sin(\theta/2)$ , giving the magnetic driving component using the gating function  $\sin(\theta/2)$  (bottom). The large connected dots denote bin averages, the vertical bars indicate the range  $\pm 1$  standard deviation from the average. Limiting to the two most quiet periods during the two solar cycles allows us to examine whether the midnight electrojet properties have changed, which would indicate differences in the level of magnetospheric activity during the selected periods.

[21] For the same level of driving solar electric field ( $E_{PAR}$ ), the electrojet current in 2009 is slightly weaker than it was in 1996. The electrojet in 2009 is also at more poleward latitudes than in 1996, indicating that the polar cap was slightly smaller for the same value of the solar wind electric field. The statistics for large values of the electric field becomes small, and thus the bin averages are only computed for values below 2 mV/m. Analyzing the independent components of the driver, the result holds true both when the data are sorted according to the solar wind speed (middle) and by the magnetic field (bottom). This indicates that indeed the magnetosphere feeds slightly less energy into the midnight sector electrojet during the year 2009 than during the previous minimum in 1996. This might be indicative of changes in the magnetotail-ionosphere coupling processes associated with, e.g., substorm activity. Similar analysis for the morning and evening sectors (not shown) reveals a similar trend, but the differences between the 2 years are much smaller and fall within the error bars.

## 5. Substorm Activity

[22] The analysis above treated the overall, continuous solar wind-magnetosphere-ionosphere coupling by analyzing the auroral electrojet characteristics and their dependence on the driving solar wind and IMF conditions. However, magnetospheric activity is not only continuous, but exhibits strong bursts, substorms, which follow periods of southward IMF and include large changes in the magnetotail field configuration and strong field-aligned currents between the magnetotail and the ionosphere [e.g., Baker *et al.*, 1996].

[23] Tanskanen [2009] examines the substorm activity using the IMAGE magnetometer chain and an automated search engine to detect substorms. These data are used here to compare the average electrojet characteristics with the number of substorms occurring during the minimum periods as well as the average size of the substorms during those periods. The search engine utilizes the  $IL$  index and defines a substorm to occur when the index decreases by more than 80 nT in 15 min, with onset defined as the time of the first sign of the drop (within 30 min of the 80 nT decrease) and substorm end defined as the time when the index recovered to 20% of the peak value. These parameters are set through comparison with manual identification and carry no particular physical meaning (see Tanskanen [2009] for details). However, as the IMAGE stations are all located in the northern hemisphere, having such set criteria does bring

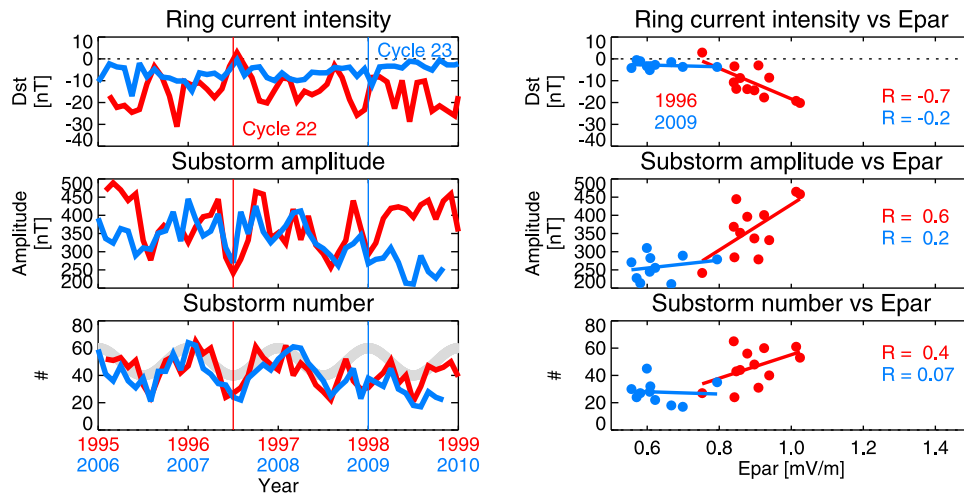


**Figure 8.** Monthly averages of the substorm activity. (left) The  $Dst$  index in nT, the substorm amplitude in nT, and the substorm number; (right) correlations of the monthly values of the driving parallel electric field  $E_{PAR} = E \sin(\theta/2)$  in mV/m with the  $Dst$  index, substorm amplitude, and substorm number during 1996 (red) and 2009 (blue).

annual variability to the search routine: In the low-conducting winter hemisphere, the field-aligned acceleration is larger leading to higher currents between the ionosphere and magnetosphere [Liou *et al.*, 2001; Newell *et al.*, 2010], and thus more events which satisfy the substorm onset criteria.

[24] Figure 8 (top left) shows the  $Dst$  index, which is a measure of the ring current intensity and thus a parameter characterizing the level of activity associated with magnetic storms. In 1996, the  $Dst$  reached a minimum activity level close to zero, but the disturbances started to increase already in 1997 when the new solar cycle began. On the other hand, the  $Dst$  values were very low during 2008 and 2009, and show a continually decreasing level of activity throughout the end of 2009. This indicates that there were only very few and small magnetic storms during that period, and that on average the ring current encircling the Earth was quite weak.

[25] In the following analysis, we concentrate on large-scale average properties during substorm periods. Therefore, we do not treat each substorm individually, but rather assume that the occurrence frequency and maximum amplitude, which are parameters that can be derived from the Tanskanen [2009] automated analysis and the average driver properties. This way we can avoid defining exact start and stop times of substorm growth, expansion and recovery phases, the transit times from the solar wind monitor to the subsolar magnetopause, and the effects of the location of the IMAGE magnetometers on the response in each individual case. Thus, the analysis below must be viewed as the overall statistical behavior of the solar wind-magnetosphere-ionosphere coupling rather than the “ground truth” during individual events.

[26] Following Tanskanen [2009] we define the substorm amplitude to be the maximum value of the  $IL$  index observed during a given substorm. Figure 8 (middle left) shows the monthly averages of the absolute values of the substorm amplitudes. There may be some hints of semiannual modulation which would produce larger substorms during equinoxes, but the tendency is clearly not as sys-

tematic as it is for the total electrojet current over all time periods shown in Figure 5. The only notable difference between the two periods (1995–1999 and 2006–2009) is that the substorm amplitude begins to decrease during 2008 and is quite low during 2009.

[27] Figure 8 (bottom left) shows monthly averages of the number of substorms. The substorm number reveals a clear annual variation with maxima during the winter months and minima during summers, which is a consequence of the selection criteria used by the substorm search engine as discussed above. During the latter part of 2008 and during 2009, the annual modulation becomes weaker and the number of substorms in 2009 is lower than it is during other times.

[28] In order to examine the large-scale coupling efficiency, we compare the years 1996 and 2009 by plotting the monthly averaged values of the  $Dst$  index, substorm amplitude and number as functions of the driving parallel electric field  $E_{PAR}$  (Figure 8, right). The data for 1996 shown in red clearly indicates a linear relationship for  $Dst$  and substorm amplitude and the driving electric field. For the substorm number, the correlation is weaker, but there is a tendency for more substorms for larger values of the electric field. During 2009, these correlations become insignificant and the  $Dst$  index as well as the substorm number and amplitude are not dependent on the level of driving.

[29] The use of monthly values in the correlations was made for two reasons: First, the maximum amplitude of the substorm is not always reached during the same hour the majority of the driving occurs. Secondly, the substorm number needs of course to be computed over a time period, and thus monthly values were selected for both quantities to make them comparable. Although not shown, the correlations computed on a hourly basis include more scatter, but the overall tendencies are the same.

[30] Figure 8 highlights the low level of average driving during 2009, but also implies that the driver dependence at these very low levels is different from that during more

average conditions (even during the solar minimum time in 1996): the substorm occurrence frequency as well as their sizes are independent of the driver. Thus, it would seem that there is a minimum number of substorms that occur even for very weak driving, and that the substorm size also reaches a minimum value that depends only weakly on the amount of driving.

[31] The analysis in Figure 8 concentrates on the two solar minimum years, 1996 and 2009. Including the full statistics over all years would increase scatter at the high end of the drivers, but convey a similar result: there is an overall linear dependence between the driver intensity and response size in the monthly averages. This linear dependence breaks when the driver intensity becomes very small; the response remains finite even for very small values of the driver. Note that in each panel, looking at the 1996 linear fit representative of also other more typical driver years, zero response is reached at a finite level of driver activity.

## 6. Auroral Observations

[32] The Finnish Meteorological Institute operates several all-sky cameras in Northern Finland and Svalbard [Syrjäsuo *et al.*, 1998]. Each camera records the auroral activity either at multiple wavelengths (green 557.7 nm, red 630.0 nm, blue 427.8 nm) or in color with a field of view of about 600 km at an altitude of 110 km. The exact spatial resolution varies as a function of the elevation angle, being of the order of 1 km near the zenith and around 10 km near the horizon. The exposure times are 0.8 s or 1 s for the green line and vary from 1.2 s to 2 s for the blue and red line images. The typical image cadence is 1–20 s, but depends on the type of instrument and its mode of operation. Images are recorded continuously and automatically throughout the dark period, which extends from September to April in mainland Fennoscandia and from November to March on Svalbard, resulting in several million images during one winter season. For quick look purposes, after each night of observation an automated routine processes keograms consisting of north-south slices of the individual green line images (see Figure 9c). As the auroras are mostly east-west aligned, keograms record most of the auroral activity.

[33] In this study, we utilize data from Ny-Ålesund (NAL, Glat 78.9°), Longyearbyen (LYR, Glat 78.2°), Kilpisjärvi (KIL, Glat 69.0°), Sodankylä (SOD, Glat 67.4°) and Hankasalmi (HAN, Glat 62.3°) stations to examine the long-term evolution of the auroras. The station locations and camera field of views are shown in Figure 2. The stations are chosen to include the northernmost and the southernmost camera stations as well as for the quality (homogeneity) of their data. The NAL and LYR stations monitor typically cusp aurora in the dayside and the poleward boundary of the oval in the nightside. The KIL and SOD stations are located at standard auroral oval latitudes, while HAN further south records auroras only during storm periods with expanded oval conditions.

[34] The digital camera network was installed during 1996–1998 such that high-quality statistical information is not available from that period from all stations relevant to this study. In 2007–2008 some stations were equipped with new cameras, either color [Partamies *et al.*, 2007] or emCCD [Sangalli *et al.*, 2010], which causes some dis-

continuities and data gaps in those time series. Thus, the most homogeneous data record covers most of the solar cycle 23, and extends through the minimum in 2007. Instrument changes noteworthy for the time period 2000–2009 are (1) the move of Hankasalmi station into Nyrölä (about 30 km west) in 2005 and (2) the change of KIL station camera into a more sensitive emCCD device in 2007. Due to the change and technical problems, there were very little high-quality data recorded at KIL in 2007. That single point in our statistics has been replaced by auroral occurrence from the Muonio station, which is located about 100 km south of Kilpisjärvi but also in the region of the main oval.

[35] To quantify the auroral activity at the selected stations, the keogram quick look data were manually examined to count the number of nights during which auroral emissions were recorded. The visual inspection was done by two researchers, who initially browsed 1 year of data together to ensure that the auroral events were identified in a consistent manner. This number of auroral nights is then scaled by the number of nights the cameras were in operation and recording data. The aim of the scaling is to remove any dependence on the length of the season and artifacts that may arise due to camera malfunctions or missing data. Figure 9b shows the sunspot number  $R$ , the latitude of the center of the westward electrojet at midnight, and the annual auroral occurrence at the five stations discussed above.

[36] Previous studies on long-term auroral occurrence in Finland suggest that the occurrence rate does not have clear correlation with the solar cycle phase [Nevanlinna and Pulkkinen, 2001]. On the other hand, the intensity of substorm activity clearly increases during the declining phase of solar activity [Nevanlinna and Pulkkinen, 1998]. Auroral activity as determined from our keogram database follows in general the trend of substorm activity: auroral occurrence is slightly higher at all stations during the declining phase years (2002–2005) than during the solar max year 2000.

[37] The northernmost stations on Svalbard (NAL and LYR) recorded approximately as frequent aurora during the solar maximum as did the instruments in the mainland (KIL, SOD, HAN). But while the auroral activity in the mainland strongly decreases in the declining phase, the auroral events remain frequent at the Svalbard latitudes. The activity decay toward the minimum in the mainland is steeper at the more southward stations. This is consistent with the poleward motion of the electrojet repeated in Figure 9b.

[38] As this statistics records only the number of auroral nights, it cannot be used to draw conclusions about the intensity of the emissions. As quiet auroral arcs fill the oval also during magnetically quiet periods, it can be expected that the latitudinal variation of the auroral occurrence is the most clear signal of solar cycle changes.

## 7. Discussion

[39] In this paper we have shown results for the auroral electrojet behavior over a 15 year period during 1995–2010. The main emphasis of the study is to examine the solar cycle and solar wind driver dependence of the electrojet activity, and to examine whether the ionosphere behaved in a qualitatively different way during the period of very low solar

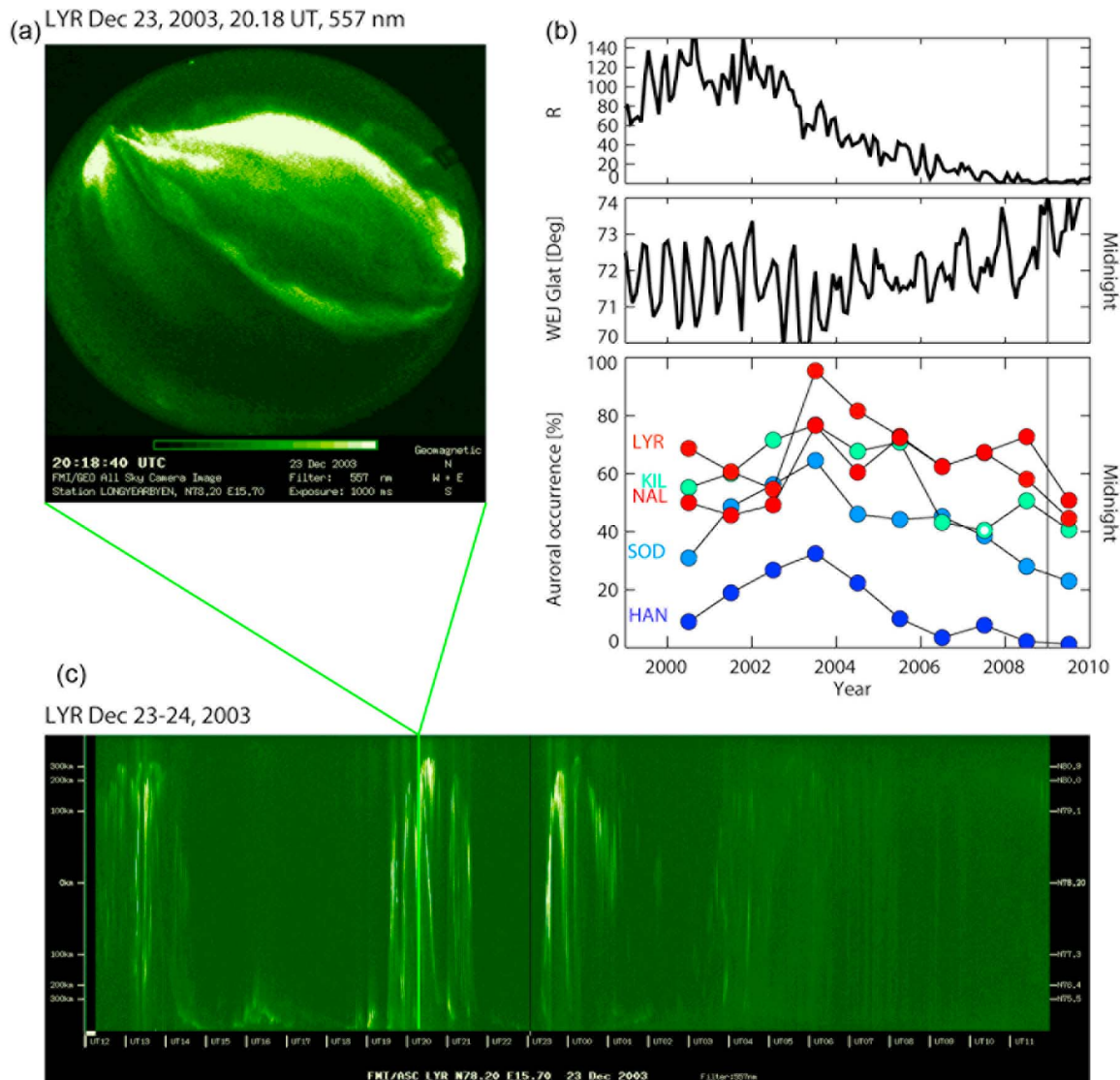


**Figure 9.** (a) An auroral image from the LYR station on 23 December 2003 in 557 nm (green line). (b) From top to bottom: sunspot number  $R$ , latitude of the westward electrojet in the midnight sector, and auroral occurrence at five stations (from north to south: LYR, NAL, KIL, SOD, and HAN). Number of nights with observed aurora is scaled by the number of observing nights at each station. The value for 2007 in the KIL data (marked by a white inner dot) is obtained from the Muonio station about 100 km further from the station because of lack of observations at the KIL station. (c) Keogram from the LYR station on 23–24 December 2003.

activity around the minimum period of cycle 23 in 2008–2009.

[40] The parameters examined consist of the total current of the westward and eastward electrojets, the center latitude of the electrojets, and the local auroral electrojet indices ( $I_U$  and  $I_L$ ) created from the magnetometer chain data in a manner similar to the global  $AU$  and  $AL$  indices. The analysis shows that the electrojet current became significantly weaker during 2008, and the semiannual variation associated with the Russell-McPherron effect disappeared; the activity remained at the level typical of solstice periods during the previous cycle. The electrojet also moved poleward by almost 2 degrees indicating that the polar cap

during the deep minimum 2008–2010 was smaller than it usually is even during solar minimum conditions.

[41] However, the driving solar wind also changed quite dramatically: the IMF magnitude was unusually small and the solar wind speed, after the high-speed streams observed in 2008, was also quite low, even below typical solar minimum conditions. Thus, the electric field imposed at the magnetopause was smaller than usual, smaller than during solar minimum conditions both during 1996 and 2007. Examining the “coupling efficiency” by taking the electrojet current divided by the driving electric field indicates that the efficiency is approximately at the same level as it was during the previous cycle. From this we can conclude that

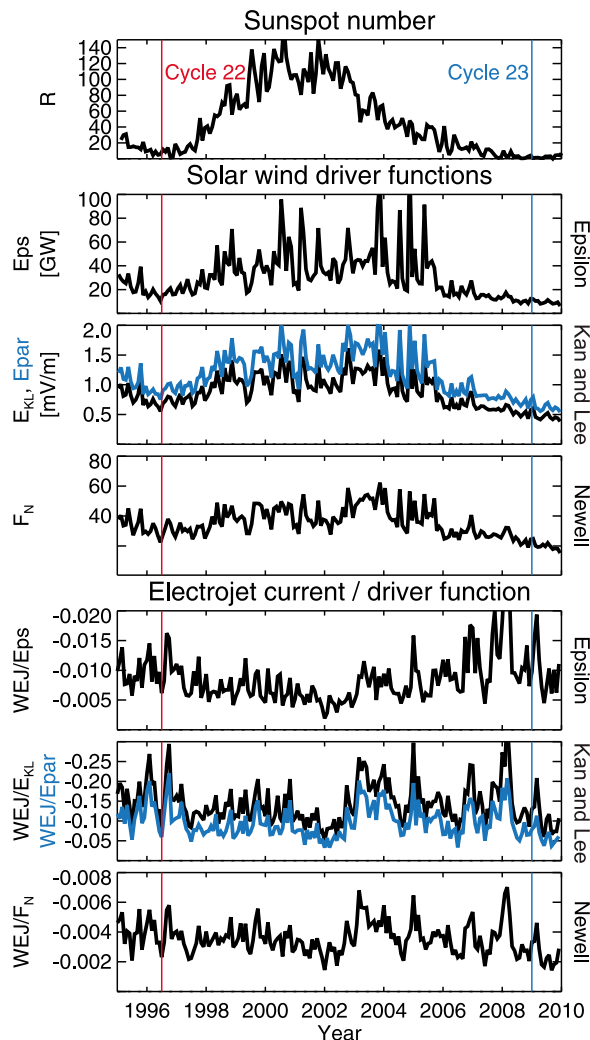


**Figure 10.** Comparison of different solar wind drivers. (top) Sunspot number  $R$ ; (middle) solar wind driver functions  $\epsilon$  parameter [Akasofu, 1981] in GW, solar wind electric field  $E_{KL}$  [Kan and Lee, 1979] (black) and  $E_{PAR}$  [Pulkkinen et al., 2009] in mV/m, and magnetic flux opened at the magnetopause  $d\Phi/dt$  [Newell et al., 2007] (not scaled); and (bottom) efficiencies computed by dividing the westward electrojet current by the driver function using hourly values.

the solar wind-ionosphere coupling processes were not affected by the very quiet solar activity.

[42] In this study, we employ the parallel electric field  $E_{PAR} = E \sin(\theta/2)$  as the driver parameter. This parameter gives the electric field along the large-scale reconnection line which forms across the dayside magnetopause. The reconnection line lies in the equatorial plane during purely southward IMF, but becomes tilted for finite IMF  $B_Y$  values. This is why the  $E_{PAR}$  is a better coupling function than the often used  $E_Y$  based on only the southward  $B_Z$  component of the IMF [Pulkkinen et al., 2010]. Other coupling functions have also been employed such as the epsilon parameter  $\epsilon = (4\pi/\mu_0)l_0^2VB^2\sin^2(\theta/2)$  [Akasofu, 1981], the Kan-Lee electric field  $E_{KL} = VB_T\sin^2(\theta/2)$  [Kan and Lee, 1979], or the rate of magnetic flux opened at the magnetopause  $d\Phi/dt = C[V^2B_T\sin^4(\theta/2)]^{2/3}$  [Newell et al., 2007], among others.

Here  $\mu_0$  is the vacuum permeability,  $l_0$  is an empirical scaling parameter often set to  $7R_E$ , and  $B_T$  is the transverse component of the IMF perpendicular to the Sun-Earth line, and  $C$  is a constant. Figure 10 compares results using different drivers. It can be noted that all drivers have qualitatively similar behavior over the solar cycle, and that the efficiencies computed using the different drivers vary in magnitude depending on the scaling of the driver function, but have qualitatively similar behavior over the entire period. Thus, this shows that our results are robust and not dependent on the choice of a particular form of the coupling function.

[43] Note that the choice of the driver function was made based on the type of analysis: we do not have results that would conclusively prove one driver parameter superior over another one. Each parameter has been derived for a different purpose, and thus have slightly different properties tuned to give best results for the question addressed by the original authors. Likewise, the absolute magnitude of the parameters depends on how they were scaled: the  $\epsilon$  parameter was scaled to amount to energy equal to dissipated by the ring current and by the ionosphere (including Joule heating and auroral precipitation), the Newell parameter only gives a functional form and is not scaled to any output. The electric field parameters only reference the external solar wind and IMF conditions with no scaling to dissipation in the magnetosphere-ionosphere system. Thus, it is inevitable that each parameter has its optimum applications and that the numbers in absolute values are not directly comparable.

[44] We examined separately the local midnight sector, which is most indicative of magnetospheric coupling processes. In this case, we only showed two years, 1996 representing the minimum activity at the end of cycle 22, and 2009 representing the weak activity following the minimum at the end of 2008. Now there are clear indications of the electrojet being weaker and at further poleward latitude during 2009 than during 1996 for the same level of solar wind driving electric field. This would indicate that the magnetosphere was at a more quiet state during 2009 than it was during 1996, thus feeding less of the energy entering from the solar wind into the ionosphere. This is a natural consequence, e.g., of very low ring current intensity, which would increase the normal component of the plasma sheet magnetic field and thus push activity further away from the inner magnetotail where it normally would reside [e.g., Milan et al., 2009].

[45] The quiet state of the magnetosphere is further emphasized when the substorm events are analyzed individually. Using the data set created by Tanskanen [2009], we computed the monthly substorm amplitude and number. Both the amplitude of the substorms and the number of substorms were quite low during 2009. Examining the correlations with the driving electric field it is clear that even during weak driving, there is a minimum number of substorms that occur, and that also the substorm size has a minimum value which is only weakly correlated with the (low level) of driving. The  $Dst$  index, which was very weak during 2009, was also almost independent of the level of solar wind driving.

[46] As the ring current in 2009 was very low, the magnetotail current sheet did not penetrate as close to the Earth

than it does when the ring current is larger. This led to the inner magnetosphere field being more dipolar than it is under more typical driving conditions. This causes the magnetic reconnection region and other associated substorm dynamics to occur further away from the Earth than under more average conditions. Under such conditions, midtail reconnection events may more often lead to large-scale substorm activity, while their size may be limited by the ability of the field-aligned currents to couple to the ionosphere.

[47] Long-term auroral records show that indeed the auroral distribution moves further poleward during low solar activity periods. The data analysis involves millions of images of which separation of cloudy images from those with real auroras is challenging [Syrjäsuo *et al.*, 2000], and thus this data set is quite unique extending over a complete solar cycle. All data sets used here, the electrojet database, the substorm database, and the auroral observations are consistent with each other, lending support to the conclusions.

## 8. Conclusions

[48] We demonstrate using auroral electrojet observations, substorm statistics, and auroral image analysis that the efficiency of the solar wind energy input to the driven ionospheric electrojets was no different during the very quiet solar activity period 2008–2009 than during other times. On the other hand, we conclude that the very quiet state of the magnetosphere as demonstrated by the *Dst* values close to zero cause the magnetosphere-ionosphere coupling to be slightly different: The substorm number stayed at a higher level than expected based on the driver intensity ( $E_{PAR}$ ). Overall, this leads to slightly weaker electrojet at further poleward latitudes in the midnight sector.

[49] **Acknowledgments.** We thank the NGDC for the solar data and the NSSDC for compiling the OMNI database of long-term solar wind observations. We thank the institutes who maintain the IMAGE Magnetometer Array. The work of E.T. was supported by the Academy of Finland grants 108518 and 128632. Tero Raita at the Sodankylä Geophysical Observatory (University of Oulu) and Stefano Massetti at IFSI-INAF (Rome, Italy) are acknowledged for the maintenance of the Sodankylä and Ny-Ålesund auroral cameras.

[50] Robert Lysak thanks the reviewers for their assistance in evaluating this paper.

## References

- Akasofu, S.-I. (1981), Energy coupling between the solar wind and the magnetosphere, *Space Sci. Rev.*, *28*, 121–190.
- Amm, O., and A. Viljanen (1999), Ionospheric disturbance magnetic field continuation from the ground to the ionosphere using spherical elementary current systems, *Earth Planets Space*, *51*, 431–440.
- Baker, D. N., T. I. Pulkkinen, V. Angelopoulos, W. Baumjohann, and R. L. McPherron (1996), The neutral line model of substorms: Past results and present view, *J. Geophys. Res.*, *101*, 12,975–13,010.
- Gibson, S. E., J. U. Kozyra, G. de Toma, B. A. Emery, T. Onsager, and B. J. Thompson (2009), If the Sun is so quiet, why is the Earth ringing?: A comparison of two solar minimum intervals, *J. Geophys. Res.*, *114*, A09105, doi:10.1029/2009JA014342.
- Häkkinen, L. V. T., T. I. Pulkkinen, R. J. Pirjola, H. Nevanlinna, E. I. Tanskanen, and N. E. Turner (2003), Seasonal and diurnal variation of geomagnetic activity: Revised *Dst* vs. external drivers, *J. Geophys. Res.*, *108*(A2), 1060, doi:10.1029/2002JA009428.
- Kan, J. R., and L. C. Lee (1979), Energy coupling function and the solar wind-magnetosphere dynamo, *Geophys. Res. Lett.*, *6*, 577–580.
- Kauristie, K., T. I. Pulkkinen, R. J. Pellinen, and H. J. Opgenoorth (1996), What can we tell about the *AE*-index from a single meridional magnetometer chain?, *Ann. Geophys.*, *14*, 1177–1185.
- Kirk, M. S., W. D. Pesnell, C. A. Young, and S. A. Hess Webber (2009), Automated detection of EUV polar coronal holes during solar cycle 23, *Sol. Phys.*, *257*, 99–112, doi:10.1007/s11207-009-9369-y.
- Lee, C. O., J. G. Luhmann, D. Odstrcil, P. J. MacNeice, I. de Pater, P. Riley, and C. N. Arge (2009), The solar wind at 1 AU during the declining phase of solar cycle 23: Comparison of 3D numerical model results with observations, *Sol. Phys.*, *254*, 155–183, doi:10.1007/s11207-008-9280-y.
- Liou, K., P. T. Newell, and C.-I. Meng (2001), Seasonal effects on auroral particle acceleration and precipitation, *J. Geophys. Res.*, *106*, 5531–5542.
- Lyatsky, W., P. T. Newell, and A. Hamza (2001), Solar illumination as cause of the equinoctial preference for geomagnetic activity, *Geophys. Res. Lett.*, *28*, 2353–2356.
- Milan, S. E., A. Grocott, C. Forsyth, S. M. Imber, P. D. Boakes, and B. Hubert (2009), A superposed epoch analysis of auroral evolution during substorm growth, onset and recovery: Open magnetic flux control of substorm intensity, *Ann. Geophys.*, *27*, 659–668.
- Nevanlinna, H., and T. I. Pulkkinen (1998), Solar cycle correlations of substorm and auroral occurrence frequency, *Geophys. Res. Lett.*, *25*, 3087–3090.
- Nevanlinna, H., and T. I. Pulkkinen (2001), Auroral observations in Finland: Results from all-sky cameras, 1973–1997, *J. Geophys. Res.*, *106*, 8109–8118.
- Newell, P. T., T. Sotirelis, K. Liou, C.-I. Meng, and F. J. Rich (2007), A nearly universal solar wind magnetosphere coupling function inferred from 10 magnetospheric state variables, *J. Geophys. Res.*, *112*, A01206, doi:10.1029/2006JA012015.
- Newell, P. T., T. Sotirelis, and S. Wing (2010), Seasonal variations in diffuse, monoenergetic, and broadband aurora, *J. Geophys. Res.*, *115*, A03216, doi:10.1029/2009JA014805.
- Partamies, N., M. Syrjäsuo, and E. Donovan (2007), Using colour in auroral imaging, *Can. J. Phys.*, *85*, 101–109.
- Pulkkinen, A., *et al.* (2003), Ionospheric equivalent current distributions determined with the method of spherical elementary current systems, *J. Geophys. Res.*, *108*(A2), 1053, doi:10.1029/2001JA005085.
- Pulkkinen, T. I., M. Palmroth, N. Partamies, H. E. J. Koskinen, T. V. Laitinen, C. C. Goodrich, J. G. Lyon, and V. G. Merkin (2009), Magnetospheric modes and solar wind energy coupling efficiency, *J. Geophys. Res.*, *115*, A03207, doi:10.1029/2009JA014737.
- Pulkkinen, T. I., M. Palmroth, H. E. J. Koskinen, T. V. Laitinen, C. C. Goodrich, V. G. Merkin, and J. G. Lyon (2010), Magnetospheric modes and solar wind energy coupling efficiency, *J. Geophys. Res.*, *115*, A03207, doi:10.1029/2009JA014737.
- Russell, C. T., and R. L. McPherron (1973), Semiannual variation of geomagnetic activity, *J. Geophys. Res.*, *78*, 92–108.
- Sangalli, L., N. Partamies, M. Syrjäsuo, C.-F. Enell, K. Kauristie, and S. Mäkinen (2010), Performance study of the new EMCCD-based all-sky cameras for auroral imaging, *Int. J. Remote Sens.*, in press.
- Syrjäsuo, M. T., *et al.* (1998), Observations of substorm dynamics using the MIRACLE network, in *Substorms-4: International Conference on Substorms-4, Lake Hamana, Japan, March 9–13, 1998*, edited by S. Kokubun and Y. Kamide, *Astrophys. and Space Sci. Libr.*, vol. 238, pp. 111–114, Terra Sci., Tokyo.
- Syrjäsuo, M. T., K. Kauristie, and T. I. Pulkkinen (2000), Searching for Aurora, paper presented at International Conference on Signal and Image Processing (SIP-2000), Int. Assoc. of Sci. and Technol. for Dev., Las Vegas, Nev.
- Tanskanen, E. I. (2009), A comprehensive high-throughput analysis of substorms observed by IMAGE magnetometer network: Years 1993–2003 examined, *J. Geophys. Res.*, *114*, A05204, doi:10.1029/2008JA013682.
- Tanskanen, E. I., T. I. Pulkkinen, and H. E. J. Koskinen (2002), Substorm energy budget near solar minimum and maximum: 1997 and 1999 compared, *J. Geophys. Res.*, *107*(A6), 1086, doi:10.1029/2001JA900153.
- Weiss, N. O., and S. M. Tobias (2000), Physical causes of solar activity, *Space Sci. Rev.*, *94*, 99–112.
- K. Kauristie, N. Partamies, E. I. Tanskanen, and A. Viljanen, Finnish Meteorological Institute, PO Box 503, FI-00101 Helsinki, Finland.  
T. I. Pulkkinen, School of Electrical Engineering, Aalto University, PO Box 13000, FI-00076 Aalto, Finland. (tuoja.i.pulkkinen@aalto.fi)